AGU PUBLICATIONS

Water Resources Research

RESEARCH ARTICLE
10.1002/2015WR016947

Capillarity and wetting of carbon dioxide and brine during drainage in Berea sandstone at reservoir conditions

Ali Al-Menhali[1,2], Ben Niu[2,3], and Samuel Krevor[1,2]

[1]Department of Earth Science and Engineering, Imperial College London, London, UK, [2]Qatar Carbonates and Carbon Storage Research Centre, Imperial College London, London, UK, [3]Department of Chemical Engineering, Imperial College London, London, UK

Key Points:
- Wettability of CO2-brine-sandstone system is insensitive to reservoir conditions
- A new method is presented to quantify shifts in effective wetting properties
- The system is strongly water wet and can be characterized by analog fluids

Correspondence to:
A. Al-Menhali,
a.al-menhali12@imperial.ac.uk

Citation:
Al-Menhali, A., B. Niu, and S. Krevor (2015), Capillarity and wetting of carbon dioxide and brine during drainage in Berea sandstone at reservoir conditions, *Water Resour. Res.*, *51*, doi:10.1002/2015WR016947.

Received 16 JAN 2015
Accepted 12 SEP 2015
Accepted article online 16 SEP 2015

Abstract The wettability of CO_2-brine-rock systems will have a major impact on the management of carbon sequestration in subsurface geological formations. Recent contact angle measurement studies have reported sensitivity in wetting behavior of this system to pressure, temperature, and brine salinity. We report observations of the impact of reservoir conditions on the capillary pressure characteristic curve and relative permeability of a single Berea sandstone during drainage—CO_2 displacing brine—through effects on the wetting state. Eight reservoir condition drainage capillary pressure characteristic curves were measured using CO_2 and brine in a single fired Berea sandstone at pressures (5–20 MPa), temperatures (25–50°C), and ionic strengths (0–5 mol kg^{-1} NaCl). A ninth measurement using a N_2-water system provided a benchmark for capillarity with a strongly water wet system. The capillary pressure curves from each of the tests were found to be similar to the N_2-water curve when scaled by the interfacial tension. Reservoir conditions were not found to have a significant impact on the capillary strength of the CO_2-brine system during drainage through a variation in the wetting state. Two steady-state relative permeability measurements with CO_2 and brine and one with N_2 and brine similarly show little variation between conditions, consistent with the observation that the CO_2-brine-sandstone system is water wetting and multiphase flow properties invariant across a wide range of reservoir conditions.

1. Introduction

The aim of carbon dioxide capture and storage is to mitigate the impacts of fossil energy consumption on climate change by safely sequestering carbon dioxide (CO_2) in deep subsurface geologic strata such as saline aquifers and depleted oil reservoirs [*Bachu et al.*, 1994; *Orr*, 2004; *Bernstein et al.*, 2007]. The importance of carbon storage in combating climate change has been highlighted in reports by the International Energy Agency [*International Energy Agency*, 2012] and the IPCC indicating that the cost of CO_2 emissions avoidance through the use of alternative energy technologies will be 150% higher in the absence of CCS [*Bernstein et al.*, 2007; *Edenhofer et al.*, 2014]. Previous and ongoing experience with industrial-scale carbon dioxide injection has come mostly from operations of enhanced oil recovery in the United States although there are a few pilot CO_2 storage projects around the world [*Global CCS Institute*, 2014]. Despite its utility for oil production and the continued development of CO_2 storage, there are longstanding uncertainties about the multiphase flow properties underlying descriptions and predictions of CO_2 migration and trapping in the subsurface.

Permeable rocks have pore sizes with length scales $10^{-6}-10^{-3}$ m. During fluid movement through constrictions at these scales, differences in interfacial energy between fluid and solid phases, $\sigma_{i,s}$ (N m^{-1}), give rise to the contact angle, θ, where $\cos\theta=(\sigma_{nw,s}-\sigma_{w,s})/\sigma_{nw,w}$. The subscripts *w*, *nw*, and *s* refer to the wetting and nonwetting fluid phases and the solid phase, respectively. The symbol $\sigma_{nw,w}$ is the interfacial tension between the two fluid phases. The interface of two fluids in a pore constriction of radius *r* (m) is thus curved and the nonwetting phase pressure, P_{nw}, is elevated relative to the wetting phase, P_w, with the difference being the capillary pressure $P_c=P_{nw}-P_w$ (Pa), described by the Young-Laplace equation,

$$P_c=\frac{2\sigma_{nw,w}\cos\theta}{r}. \quad (1)$$

In the complex pore structures of geologic media, capillarity results in an organization of fluids into relatively large or small constrictions depending on their wetting state. This in turns results in the unique

properties of multiphase flow in a porous media in which fluid permeability and pressure are dependent on the fluid saturation in the rock. In this work, we characterize the capillarity of a system through the characteristic capillary pressure-saturation relationship of that system.

This is of major practical importance in the petroleum industry, environmental waste remediation, and subsurface hydrology [*Craig*, 1971; *Anderson*, 1987]. It is key to understanding the movement of large volumes of CO_2 injected into subsurface reservoirs. The relationships between the capillarity of a geologic system, and the saturation and permeability of the fluids has a direct bearing on the migration speed and reservoir sweep of a CO_2 plume [*Nordbotten and Dahle*, 2011; *Golding et al*., 2011, 2013], immobilization through capillary trapping [*Juanes et al*., 2006; *Hesse et al*., 2008] and is used directly in assessments of the capacity of a storage site to contain CO_2 over geologic timescales [*Szulczewski et al*., 2012; *Warwick et al*., 2013].

In this investigation, we have sought to resolve an outstanding uncertainty about the wetting properties of CO_2-brine rock systems so far as they impact the capillarity during drainage, when CO_2 is displacing a resident brine. This will determine the extent to which the multiphase flow of CO_2-brine systems will be effected at scales relevant to CO_2 migration in the reservoir.

Both drainage and imbibition processes are important for a full description of multiphase flow and for CO_2 storage. We have first focused on drainage in this work, however, as it is the primary displacement process taking place while CO_2 is injected into a reservoir. For industrial storage projects, this period will last for decades and will be the key displacement process to model during the highest risk stages of the injection projects [*Hesse et al*., 2008; *Szulczewski et al*., 2012]. For latter stages of storage projects, after injection has ceased and when the CO_2 plume is migrating, both drainage and imbibition processes are taking place simultaneously, albeit at different locations in the plume [*Doughty and Pruess*, 2004], and for these observations of capillarity during imbibition will be important.

From equation (1), it is apparent that the wetting properties of a system will serve to strengthen or weaken capillarity and this indeed is the primary interest of research on wettability in application to CO_2 storage. In a porous rock, this weakening generally applies, although the picture is more complex. An extensive review of the impacts of the wetting state on capillarity in reservoir rocks was given in *Anderson* [1987]. While equation (1) was initially proposed as a way to scale measurements of capillary characteristics of rocks among various fluid pairs [*Purcell*, 1949], it has been shown that it does provide an accurate scaling for consolidated rocks so far as the contact angle is concerned [*Dumore and Schols*, 1974; *Kruyer*, 1958; *De Witt and Schölten*, 1975; *Swanson*, 1985; *Good and Mikhail*, 1981; *Morrow*, 1976; *McCaffery and Bennion*, 1974; *Anderson*, 1987].

Decreasing the strength of the wetting state within a given rock manifests as a weakening of capillarity during drainage, but only after the wetting state has been significantly weakened from strongly wetting [*Morrow*, 1976; *Anderson*, 1987]. In other words, small differences in the affinity of fluids for the solid can give rise to strong capillarity in real rocks, and it is only when fluids have relatively similar solid interfacial energies that effects on multiphase flow are observed. This is primarily due to the options available for energy minimization and the configuration of contact lines provided by complex geometries at rock pore walls [*Decker et al*., 1999]. Further complicating observations for real geologic media, wettability can be distributed throughout a rock heterogeneously because of the distribution of specific minerals or the presence of hydrocarbon films [*Salathiel*, 1973; *Jadhunandan and Morrow*, 1995]. In the absence of a definitive understanding of the wetting state of a system, there is significant uncertainty around the capillary-dominated processes of multiphase flow.

The primary concern of this work is that several investigations into the wetting properties of CO_2-brine rock systems have resulted in ambiguous determination of the wetting state [*Chiquet et al*., 2007; *Espinoza and Santamarina*, 2010; *Jung and Wan*, 2012; *Wang et al*., 2012; *Kim et al*., 2012; *Broseta et al*., 2012]. This outstanding issue has been summarized in a recent review paper by *Iglauer et al*. [2015]. Most observations have suggested that CO_2 is nonwetting on minerals unaltered by the presence of a hydrocarbon but differ in conclusions about the strength of the wetting state and sensitivity to pressure, temperature and salinity, and among minerals prevalent in reservoir rocks.

Observations of the contact angle between a sessile or pendant drop of fluid and a polished mineral surface have been the most common technique employed and have been reported for a range of pressure (1–10 MPa), temperature (25–50°C), and brine salinity (0–5 mol kg^{-1}). Increasing brine salinity has been

Table 1. Experimental Conditions Used in This Study are Shown for Both Capillary Pressure Tests, Indicated by P_c in the Experiment Type Column, and Relative Permeability Tests, Indicated by k_r[a]

Experiment No.	Type	Nonwetting Fluid	Salinity (mol kg^{-1})	Temperature/Pressure (°C)/(MPa)	IFT[b] (mN m^{-1})	Range[c] (mN m^{-1})
1a, 1b	P_c	$scCO_2$	0	50/10	36	30–32[d,g]
2	P_c	$scCO_2$	1	50/10	37	32–33[f,h]
3	P_c	$scCO_2$	3	50/10	41	35–38[e,f]
4	P_c	$scCO_2$	5	50/10	44	46[e]
5	P_c	$liqCO_2$	0	25/10	34	28–30[d,g]
6	P_c	$liqCO_2$	3	25/10	38	29[f]
7	P_c	gCO_2	0	50/5	47	41–48[d,g]
8a,8b	P_c	$scCO_2$	0	50/20	30	24–29[e,g]
9	P_c	$scCO_2$	0.3	50/20	30	N/A[i]
10	P_c	N_2	0	25/10	67	
11	k_r	$scCO_2$	0	50/10	36	
12	k_r	$scCO_2$	3	50/10	41	
13	k_r	N_2	0	25/10	67	

[a]The interfacial tension used for scaling in this work, calculated from the correlation in *Li et al.* [2012], is shown along with the range of values at similar conditions reported in other literature.
[b]CO_2 data from *Li et al.* [2012]. N_2 data from *Yan et al.* [2001].
[c]Excluding *Li et al.* [2012].
[d]*Chun and Wilkinson* [1995].
[e]*Bachu and Bennion* [2009].
[f]*Chalbaud et al.* [2009].
[g]*Georgiadis et al.* [2010].
[h]*Tokunaga et al.* [2013].
[i]Test with NaI.

observed to decrease the water wetting in observations reported by *Espinoza and Santamarina* [2010]; *Jung and Wan* [2012]; *Kim et al.* [2012]. It has been observed to have little effect, however, in studies by *Chiquet et al.* [2007] and *Broseta et al.* [2012]. A decrease in the water wetting with increasing CO_2 pressure has been observed on quartz and mica by *Chiquet et al.* [2007]; *Jung and Wan* [2012]; *Broseta et al.* [2012]; *Saraji et al.* [2013]; and *Iglauer et al.* [2014]. However, observations reported in *Espinoza and Santamarina* [2010] and *Farokhpoor et al.* [2013] saw little influence of CO_2 pressure. The observations reported in *Wang et al.* [2012] were sensitive to pressure and temperature, but without a discernible trend. The reported effects were generally stronger during imbibition processes, but sensitivity was also seen in brine receding contact angles representative of drainage. The work reported in *Iglauer et al.* [2014] also showed that the observations were sensitive to sample preparation procedures and it was suggested that this was the main source of the discrepancies.

Contact angles measured in sessile and pendant drop experiments with the range of uncertainty reported cannot be used directly to assess the strength of capillarity and the impact on multiphase flow. For this

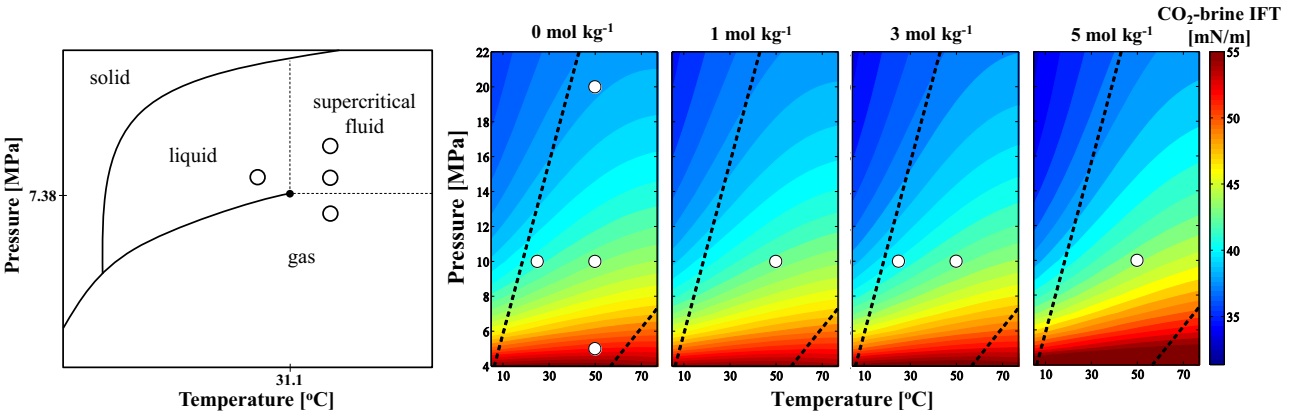

Figure 1. (left) A carbon dioxide phase diagram with the experimental conditions shown by the white circles. (right) Experimental conditions are plotted on a map of CO_2-brine IFT (contours) [*Li et al.*, 2012] as a function of pressure and temperature at the brine salinities (NaCl) used in this study. The dotted black lines represent the range of global geothermal and hydrostatic gradient for target CO_2 storage reservoirs worldwide after *Bachu* [2003].

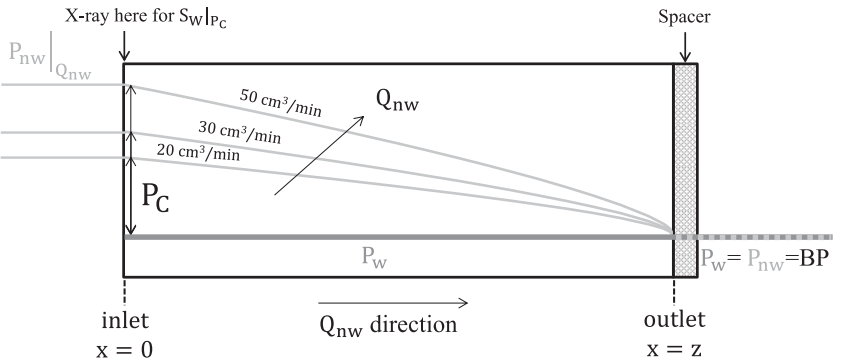

Figure 2. A schematic of the main principles of the technique used in this work. The technique is described in section 2.4. A spacer was used to create a reservoir for the outlet boundary condition. Reservoir simulation was used to confirm pressure profiles were consistent with the assumptions described in section C. Simulation results showing pressures in the CO_2 and aqueous phases are shown in the figure with the corresponding flow rates, Table 2. The text BP refers to the back pressure.

reason, wettability assessments used in industry primarily interested in fluid flow use the Amott and U.S. Bureau of Mines (USBM) wettability tests [*Amott*, 1959; *Donaldson et al*., 1969; *Jerauld and Rathmell*, 1997; *Iglauer et al*., 2012], which are based directly on evaluations of the capillary pressure characteristic curve (USBM) or the relative fluid production after spontaneous and forced imbibition (Amott), primarily controlled by the capillary pressure characteristic curve. They are considered superior to the contact angle method when the wetting state is unknown, e.g., in the case of a native state core [*Cuiec*, 1975] or in the present case of CO_2-brine systems.

This approach has been adopted for this study and has also been adopted by two groups investigating similar issues with CO_2-brine systems in unconsolidated pure quartz sand [*Plug and Bruining*, 2007; *Tokunaga et al*., 2013]. Observations reported by *Plug and Bruining* [2007] of drainage and imbibition capillary pressure curves for gaseous and supercritical CO_2-water showed little impact of the wetting state on the drainage process in a sand pack with permeability $k \approx 10^{-10}$ m^2. Capillarity measured with CO_2 was indistinguishable from measurements made with N_2. The imbibition process, however, suggested that the supercritical CO_2 system was less strongly water wet than the gaseous CO_2 and N_2 systems. Observations reported in *Tokunaga et al*. [2013] using a sand pack with an order of magnitude lower permeability ($k \approx 10^{-11}$ m^2) found both drainage and imbibition capillarity to be strongly affected by pressure. The supercritical system approached an intermediate wetting state with weak capillarity as pressure varied from 8.5 to 12.0 MPa.

Observations of capillarity during drainage in consolidated rocks including Berea sandstone have been reported in *Pentland et al*. [2011]; *Pini et al*. [2012]; and *Pini and Benson* [2013]. Those studies were not designed to assess the impact of varying reservoir conditions but the observations suggested that drainage capillary pressure curves were not affected by variations in the wetting state in the comparison of a supercritical CO_2-brine system to a decane-brine system [*Pentland et al*., 2011], between a liquid and supercritical CO_2 system [*Pini et al*., 2012] and gaseous CO_2 in comparison with supercritical CO_2 and a N_2-brine system [*Pini and Benson*, 2013].

Table 2. Flow Rates and Capillary Numbers for the Capillary Pressure Experiments

Experiment	q_{CO_2}/(cm^3 min^{-1})	N_c
1	0.5–50	$2.8\times10^{-8}-2.8\times10^{-6}$
2	0.5–45	$2.6\times10^{-8}-2.4\times10^{-6}$
3	0.5–45	$2.4\times10^{-8}-2.2\times10^{-6}$
4	0.5–45	$2.3\times10^{-8}-2.0\times10^{-6}$
5	0.5–30	$7.6\times10^{-8}-4.6\times10^{-6}$
6	0.5–40	$6.7\times10^{-8}-5.4\times10^{-6}$
7	0.5–30	$1.3\times10^{-8}-7.7\times10^{-7}$
8	0.5–25	$8.0\times10^{-8}-4.0\times10^{-6}$
9	0.5–25	$8.0\times10^{-8}-4.0\times10^{-6}$
10	0.5–50	$1.0\times10^{-8}-1.0\times10^{-6}$
11	0.75–15	$4.2\times10^{-8}-8.3\times10^{-7}$
12	0.75–15	$3.7\times10^{-8}-7.3\times10^{-7}$
13	0.75–15	$1.5\times10^{-8}-3.1\times10^{-7}$

Beyond capillarity, *Egermann et al*. [2006] used observations of unsteady state drainage of CO_2 displacing brine at a range of pressures, temperatures, and brine salinities to evaluate effects of sensitivity to the wetting state. It was found that characterizing capillary pressure and relative permeability with mercury-air and N_2-brine fluid pairs, respectively, were sufficient to predictively model the displacements with CO_2 (production and pressure time series) so long as the variation in thermophysical properties were

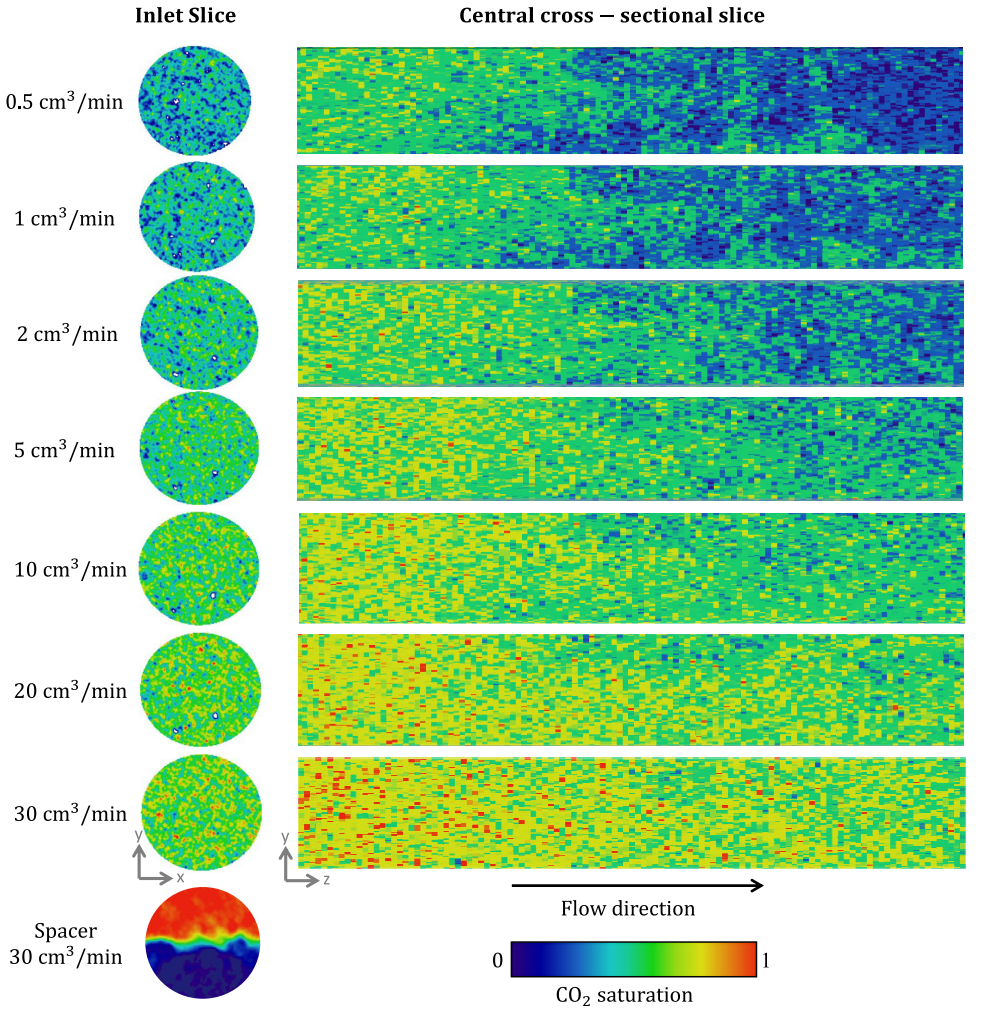

Figure 3. Vertical-horizontal saturation maps for Experiment 7, with gaseous CO_2, along the central cross-sectional slice. These saturation maps confirmed that CO_2 was distributed uniformly with no dissolution, gravity segregation, or impacts of rock heterogeneity. A cross-sectional image of the spacer located between sample and outlet endcap showed the fluid phases inside the spacer and confirmed a continuous water phase even at high-flow rates.

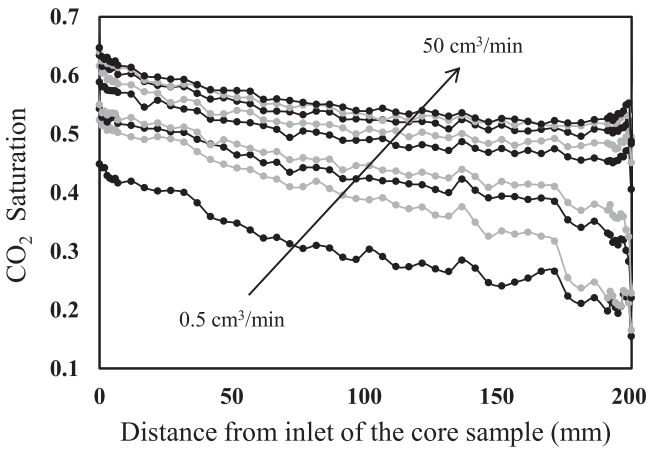

Figure 4. The slice-averaged CO_2 saturation profiles along the length of the core at different injection flow rates during Experiment 1, CO_2-water at 10 MPa and 50°C.

taken into account. It was further identified that CO_2 entry pressures scaled with interfacial tension, indicating that drainage was water wet. Using observations of relative permeability alone, *Pini and Benson* [2013] found the system to be consistent with the water-wet N_2-water system whereas *Levine et al.* [2014] found CO_2-brine systems to be less strongly water wet than N_2 systems, but with the CO_2 still acting as the nonwetting phase.

In this work, a core flood capillary pressure test [*Ramakrishnan and Cappiello*, 1991; *Lenormand et al.*, 1993; *Fordham et al.*, 1993; *Pini et al.*, 2012; *Pini and*

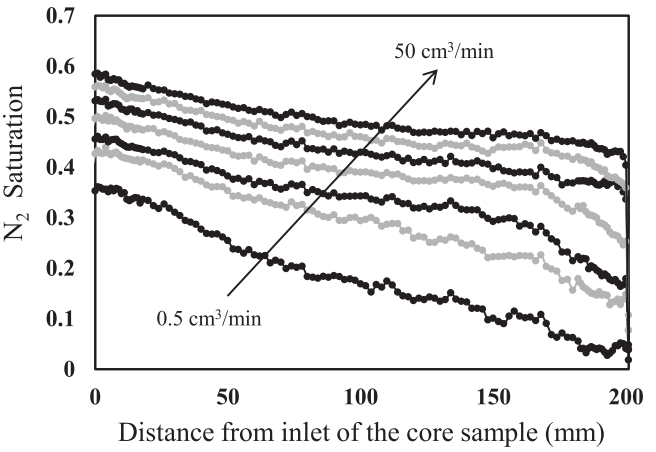

Figure 5. The slice-averaged N_2 saturation profiles along the length of the core at different injection flow rates during Experiment 10, N_2-water at 10 MPa and 25°C.

Benson, 2013] was used to characterize the capillary pressure characteristic curve of the CO_2-brine-sandstone rock system. A range of conditions were tested to assess whether CO_2 flowed as a nonwetting fluid during drainage, and if this was sensitive to reservoir conditions of pressure, temperature, and brine salinity. We performed the tests in a single Berea sandstone at eight conditions systematically varying pressure, temperature, and brine salinity. To assess the wetting state of the CO_2 systems, a test was also performed with the N_2-water system, known to be water wet in Berea sandstone [*Wu and Firoozabadi*, 2010a, 2010b].

The conditions were chosen to cover a range representative of subsurface conditions in real target storage reservoirs. They also allowed for observations of capillarity with CO_2 as a gaseous, low–density, and high-density supercritical fluid, corresponding to system variations reported in the literature to have an impact on the wetting state. Relative permeability characterization tests were also performed at two conditions with CO_2-brine systems and with the N_2-water system to show the impact of the wetting state on multiphase flow. Finally, imbibition relative permeability observations were combined with observations of the residual trapping characteristic reported in a previous study [*Niu et al.*, 2015] to provide a preliminary indication of how the drainage results reported extend toward imbibition processes.

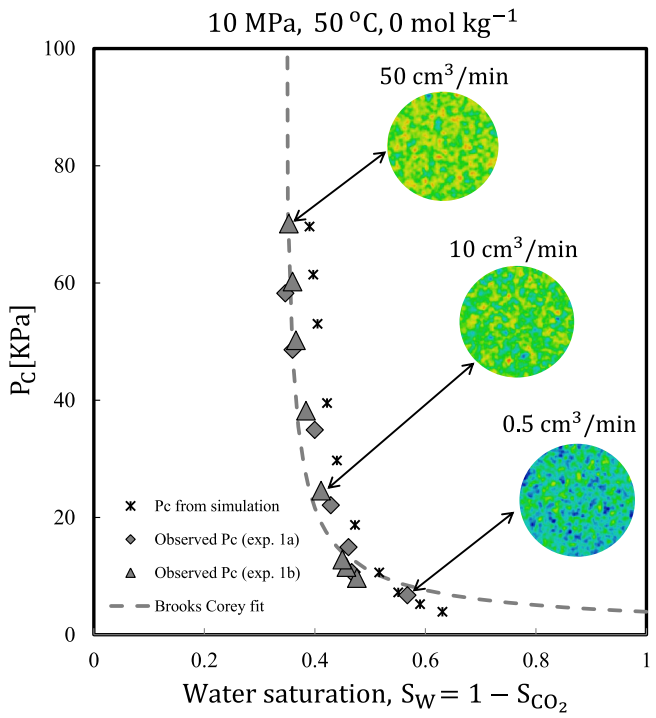

Figure 6. Results from Experiment 1, a CO_2-water capillary pressure observation, showing the inlet slice saturations associated with three of the points in Experiment 1b. The solid symbols are the observations, the curve represents the best fit Brooks-Corey curve, and the stars represent the anticipated results from the simulation model that led to the choice of drainage flow rates.

2. Materials and Methods

2.1. The Rock Sample

A single homogeneous 20.32 cm long, 3.81 cm diameter Berea sandstone core sample was used for all of the tests performed in this study. Berea sandstone is an outcrop rock from the United States which is widely used in studies as a benchmark and for its utility in making comparisons with other studies of petrophysics [*Oak et al.*, 1990; *Wu and Firoozabadi*, 2010a; *Pentland et al.*, 2011]. The sample was heated at 700°C for 4 h as is standard to stabilize swelling clays that can otherwise lead to permeability changes during tests. The faces of the core were machined flat to ensure good contact with the endcaps. The sample was vacuum dried in air at 70°C overnight before each test. The absolute permeability of the sample to water was 212 mD with an average porosity of 21% as measured by X-ray computed tomography (CT) scanning.

Table 3. Best Fit Brooks-Corey Parameters for the Capillary Pressure Characteristic Curve Tests[a]

Experiment	P_e/kPa	$S_{w,irr}$
1	3.9 ± 1.5	0.34
2	4.3 ± .2	0.38
3	4.6 ± .2	0.37
4	7.7 ± .4	0.37
5	3.9 ± .4	0.40
6	3.9 ± .8	0.40
7	5.9 ± .1	0.29
8	2.7 ± .3	0.34
9	4.5 ± .1	0.51
10	8.1 ± .2	0.36

[a]For all experiments, $\lambda = 1.4$ was held fixed. Uncertainty bounds on the entry pressure are two times the standard error of the least products regression. The standard error on the values of $S_{w,irr}$ were all less than 0.01.

The capillary pressure characteristic curve of several samples of the Berea sandstone were initially characterized using the mercury injection capillary pressure test (MICP). The skeletal density of the sample was measured with helium pycnometer on a subsample (0.8 cm^3) that was cut from a section adjacent to the inlet face of the core sample and subsequently characterized by MICP using an AutoPore IV from Micromeritics. The pressure range measured was from vacuum to 240 MPa. The capillary pressure and pycnometery measurements were performed on several samples. Following a protocol described in *Pini and Benson* [2013], the mercury saturation in the MICP data was corrected using the true skeletal density obtained from the helium pycnometer. The true water porosity was measured by X-ray CT of the inlet face of the core.

2.2. Test Conditions

The test conditions are shown in Table 1. Carbon dioxide and nitrogen were used as the nonwetting phases in the coreflooding experiments both with 99.9% purity (BOC Industrial Gases, UK). The wetting phase fluids used were deionized water or NaCl brine. The brine solutions were made of deionized water and NaCl with total salt molality ranging from 0 to 5 mol kg^{-1}.

The values of interfacial tension of the fluid pairs were used to scale the capillary pressure measurements for the assessment of wettability (section 2.5). Much of the analysis is based on values of interfacial tension calculated from the empirical correlation for the CO_2-brine system reported by *Li et al.* [2012], shown in Figure 1 and included in Table 1. We also include in Table 1 the range of values reported in the literature for conditions similar to those used in this work [*Chun and Wilkinson*, 1995; *Bachu and Bennion*, 2009; *Chalbaud et al.*, 2009; *Georgiadis et al.*, 2010; *Tokunaga et al.*, 2013]. At some conditions, the values reported by *Li et al.* [2012] are significantly higher and outside of the range of values reported by the other groups. This is discussed in *Georgiadis et al.* [2010] where the discrepancy was attributed to fluid contamination in the measurements that resulted in lower values. Thus we evaluated the impact of the variation in reported interfacial tension on the interpretation of the measurement. This is discussed in detail in the results section 3. In most cases, it made little qualitative difference to the conclusions.

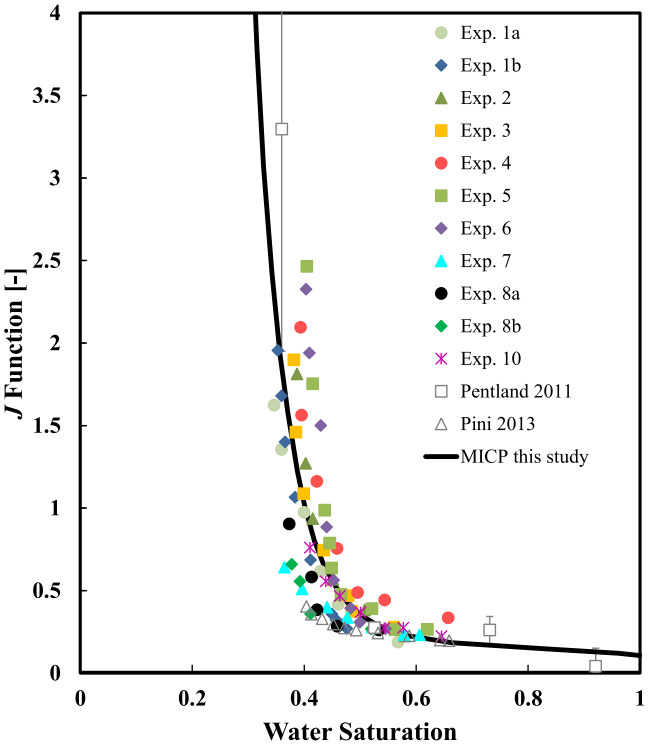

Figure 7. Data from all of the experiments scaled by the dimensionless *J*-function without any adjustments for the wetting state. The adjusted MICP curve is shown along with observations in Berea sandstone reported in *Pentland et al.* [2011]; *Pini and Benson* [2013] for comparison. Experimental conditions are listed in Table 1.

In one test, Experiment 9, the wetting phase solution was deionized water with 5 wt% of the X-ray dopant NaI. This was done to confirm the accuracy of the saturation observations without using the dopant [*Al-Menhali et al.*, 2015]. Because the interfacial properties were less well constrained for NaI, the other experiments were performed using NaCl solutions.

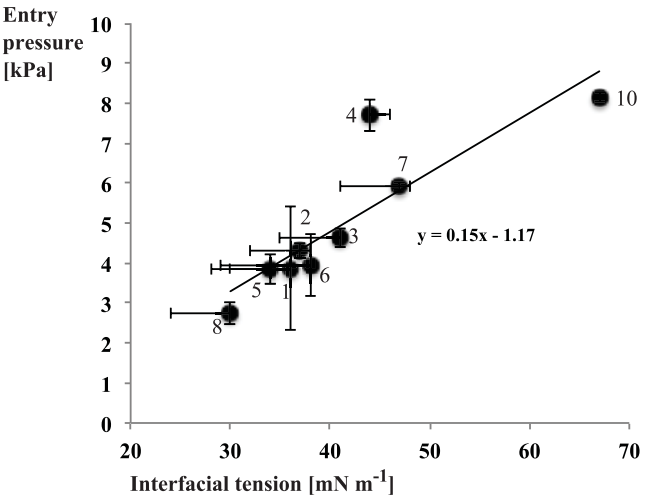

Figure 8. Best fit entry pressure, Table 3, plot against the interfacial tension, Table 1. The data points use the interfacial tension obtained from the correlation of *Li et al.* [2012] while the horizontal whiskers show the range of reported values. Vertical whiskers are the uncertainty associated with the fit entry pressures reported in Table 3. The numbers next to the data points indicate the experiment number.

2.3. Core-Flooding Experimental Setup

Capillary pressure and relative permeability measurements were conducted using a two fluid phase core flooding system shown in Figure A1 in Appendix A. The experimental setup was designed to replicate in situ temperature and pressure conditions of up to 120°C and 30 MPa. The system included, six pumps (Teledyne Isco, Model 500D, and 100DX), a two phase separator, two high-accuracy pressure transducers (Oil-filled Digiquartz Intelligent transmitter, Model 410K-HT-101), and a Pheonix Instruments core holder wrapped in a silicone heating tape with temperature measured in the confining fluid. The setup was a closed loop system which allowed for a pre-equilibration of CO_2 and brine prior to initiation of drainage in the rock core, creating an immiscible displacement, and allowed fluids to be coinjected into the core sample at controlled rates (constant rate injection). The core holder was positioned horizontally through a medical X-ray CT scanning instrument refurbished for petrophysical work (Universal Systems, HD-350).

2.4. Measuring the Capillary Pressure Characteristic Curve

We used a core flooding test to measure the capillary pressure at the inlet of the rock core during drainage [*Ramakrishnan and Cappiello*, 1991; *Fordham et al.*, 1993; *Lenormand et al.*, 1993; *Pini et al.*, 2012; *Pini and Benson*, 2013]. A schematic showing the principles of the method is shown in Figure 2. A detailed description of the startup and operation of the experiment is provided in Appendix A and summarized here.

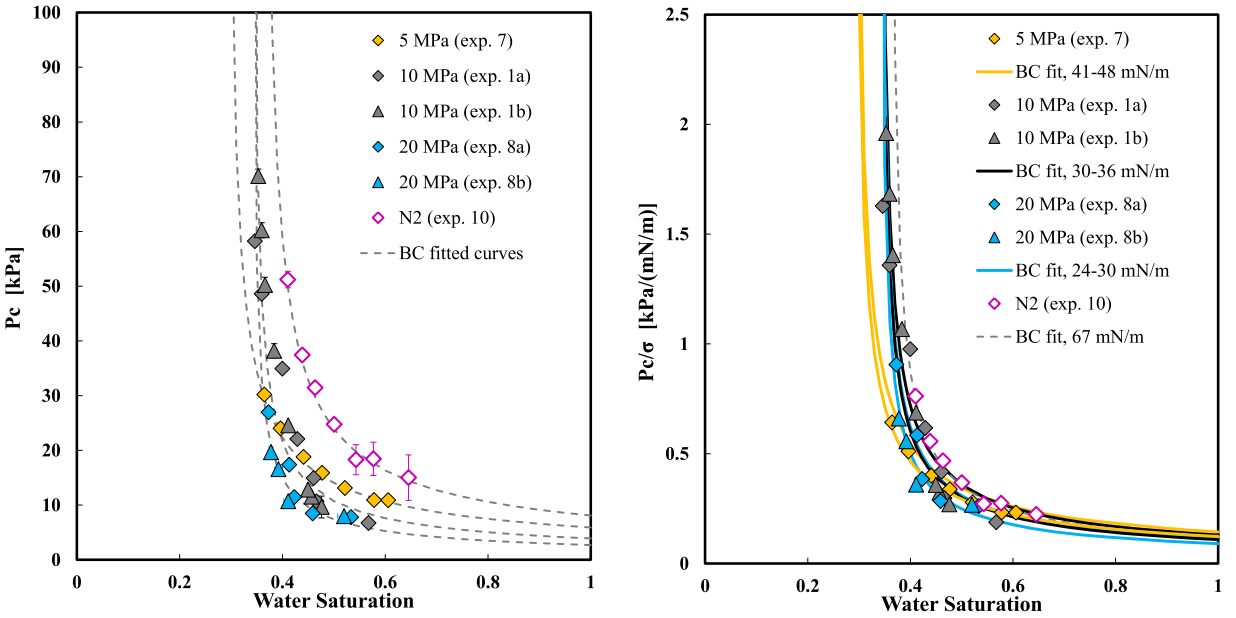

Figure 9. Results showing the effect of pressure variation on capillarity.

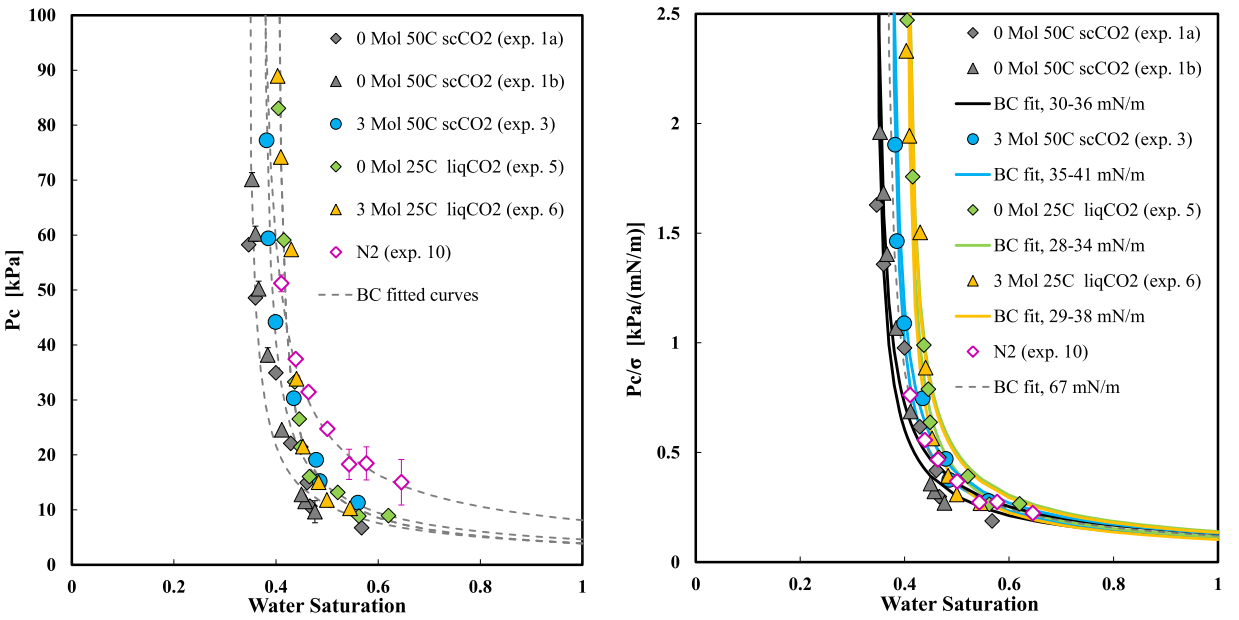

Figure 10. Results showing the effect of temperature variation on capillarity.

To make the measurements, CO_2 was injected into an initially water or brine-saturated core sample at a steady and low-flow rate. The pressure drop across the sample set the capillary pressure at the inlet face of the core where the saturation was measured using an X-ray CT scanner using standard techniques [*Akin and Kovscek*, 2003] with a detailed procedure provided in Appendix B. To ensure a reservoir of brine at the outlet boundary [*Ramakrishnan and Cappiello*, 1991], a spacer was used at the downstream end of the core (Figure 2). A capillary pressure curve was constructed by repeating these measurements at increasing CO_2 flow rates.

Flow rates were initially selected using the aid of a numerical simulation of the core flood. This is detailed in Appendix C. Example simulation results of pressure profiles of CO_2 along the length of the core at various fluid flow rates are shown in Figure 2. The injection flow rates ultimately used for the experiments varied

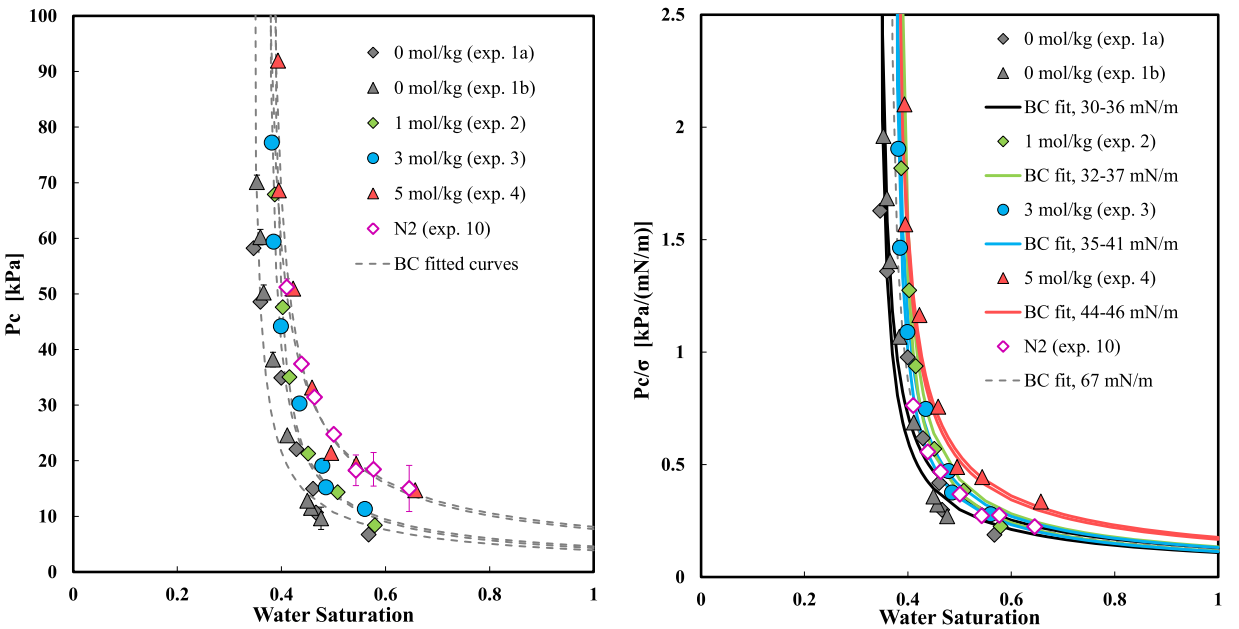

Figure 11. Results showing the effect of water salinity on capillarity.

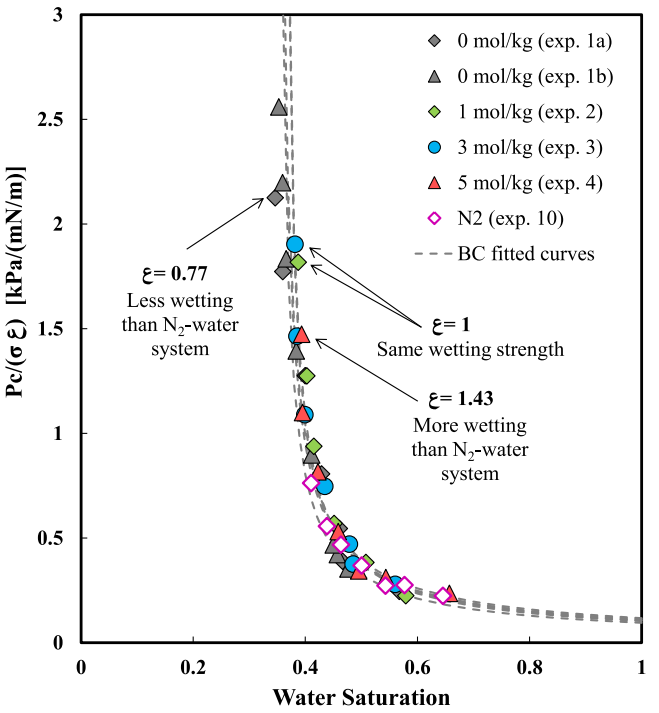

Figure 12. Results showing the effect of water salinity with capillary pressure curves scaled by interfacial tension and ξ to quantify potential impacts of wettability variations. Nitrogen-water capillary pressure was used as a wetting reference. The values of ξ applied in this graph are displayed in Table 4.

from 0.5 up to 50 mL min^{-1}. The range of dimensionless capillary number, $N_c = v\mu/\sigma$, combining the flow velocity v, viscosity μ, and interfacial tension σ, is shown for each experiment in Table 2. The values of N_c for the highest flow rates applied in this study ranged between $10^{-7}$and 10^{-6}. These capillary numbers were below the critical value for ensuring a capillary dominated distribution of fluids in the pores. For Berea sandstone, this has been observed to be in the range $N_c > 10^{-5}-10^{-4}$ [*Taber*, 1969; *Foster*, 1973; *Gupta and Trushenski*, 1979].

2.5. Assessing Wetting State Variation From Capillary Pressure Observations

The Brooks-Corey model was fit to the capillary pressure observations [*Brooks and Corey*, 1964],

$$P_c = P_e\left(\frac{S_w - S_{w,irr}}{1 - S_{w,irr}}\right)^{-1/\lambda}. \quad (2)$$

The entry pressure is given by P_e (Pa) (i.e., the minimum pressure required for the entry of CO_2 into the pores of the rock), the subscript w represent the wetting phase, the subscripts irr represents the irreducible saturation, and λ tunes the curvature of the model.

To assess the impact of the wetting state, a curve was first fit to the N_2-water data to obtain a value for λ. Then curves were fit to the CO_2-brine data using P_e and $S_{w,irr}$ as fitting parameters while holding λ constant. All fits were performed using least products regression, considering both pressure and saturation observations as prone to error. Finally, these curves were scaled by the values of interfacial tension in Table 1. Plots of P_c/σ against S_w were used as the basis for identifying the impact of reservoir conditions on wettability [*Morrow*, 1976; *Plug and Bruining*, 2007; *Tokunaga et al.*, 2013].

The dimensionless J-function was also used to scale capillary pressure curves to compare the observations made for this work with data reported in the literature,

$$J(S_w) = \frac{P_c(S_w)\sqrt{k/\phi}}{\sigma}. \quad (3)$$

Table 4. Wettability Multiplier (ξ) Values Used for Scaling CO_2 Capillary Pressure Curves to the N_2 Capillary Pressure Curve as a Water Wet Reference

Experiment	Wettability Index
1	0.77
2	1
3	1
4	1.43
5	1
6	1
7	0.82
8	0.78
10	1

3. Results and Discussion

Figures 3–6 show examples of the data collected for each of the capillary pressure tests. Two and three-dimensional saturation maps of the type shown in Figure 3 confirmed that gravity segregation, fluid phase mass transfer, and rock heterogeneity did not have an impact on the fluid distribution throughout the core, validating assumptions underlying the test. Similarly, observations of the fluids in the outlet spacer (Figure 3) confirmed that the downstream end of the rock core remained in contact with the water reservoir at all of the flow rates.

Table 5. Brooks-Corey Parameters for Curves Fit to Drainage Relative Permeability Experiments[a]

Experiment	$S_{w,irr}$	$S_{nw,r}$	$k_{r,w}(S_{nw,r})$	$k_{r,nw}(S_{w,irr})$	n_w	n_{nw}
11	0.2	0	1	0.8	5.3	3.8
12	0.2	0	1	0.8	5.3	3.6
13	0.2	0	1	0.8	5.3	3.1

[a]The only parameters used to fit the curves were n_w and n_{nw}. The endpoint parameters were assumed. See text for details.

The slice-averaged saturation profiles along the length of the core shown in Figure 4 for a CO_2 test and Figure 5 for a N_2 test showed the negative saturation gradient expected from the capillary end effect. In this case, the N_2 experiment exhibited a higher capillary end effect corresponding to the lower viscosity of N_2 compared with CO_2 at these test conditions.

Capillary pressure-saturation pairs for Experiment 1 are shown in Figure 6 alongside saturation maps from the inlet slice of the core. Also shown are the anticipated capillary pressure observations from the numerical simulation which used the MICP curve, scaled by interfacial tension, as an input to select the flow rates.

The pore-size distribution index obtained from the Brooks-Corey model fit to the N_2-water test, equation (2), was $\lambda = 1.39 \pm .03$. For the CO_2 tests, best fit Brooks-Corey curves were obtained using the entry pressure, P_e, and the irreducible water saturation, $S_{w,irr}$ as the fitting parameters, but maintaining $\lambda = 1.4$. Best fit values for all of the capillary pressure tests are reported in Table 3. All of the data are plotted scaling using the dimensionless *J*-function, equation (3), in Figure 7 with the values of interfacial tension calculated from the correlation of *Li et al.* [2012]. In this scaling, no adjustments were made using a term, e.g., $\cos\theta$, reflecting the wetting state.

A plot of the best fit entry pressures from Table 3 against the interfacial tension is shown in Figure 8. The data show a positive correlation with a linear proportionality constant in the range of what would be expected for, e.g., 10 μm pore throats and a relationship with interfacial tension only. Experiment 4, with the highest salinity brine was a significant outlier, while entry pressures obtained for Experiments 1 and 6 were lower than expected for the interfacial tension and could indicate a small effect of the wettability state. These variations are discussed in more detail in the following sections.

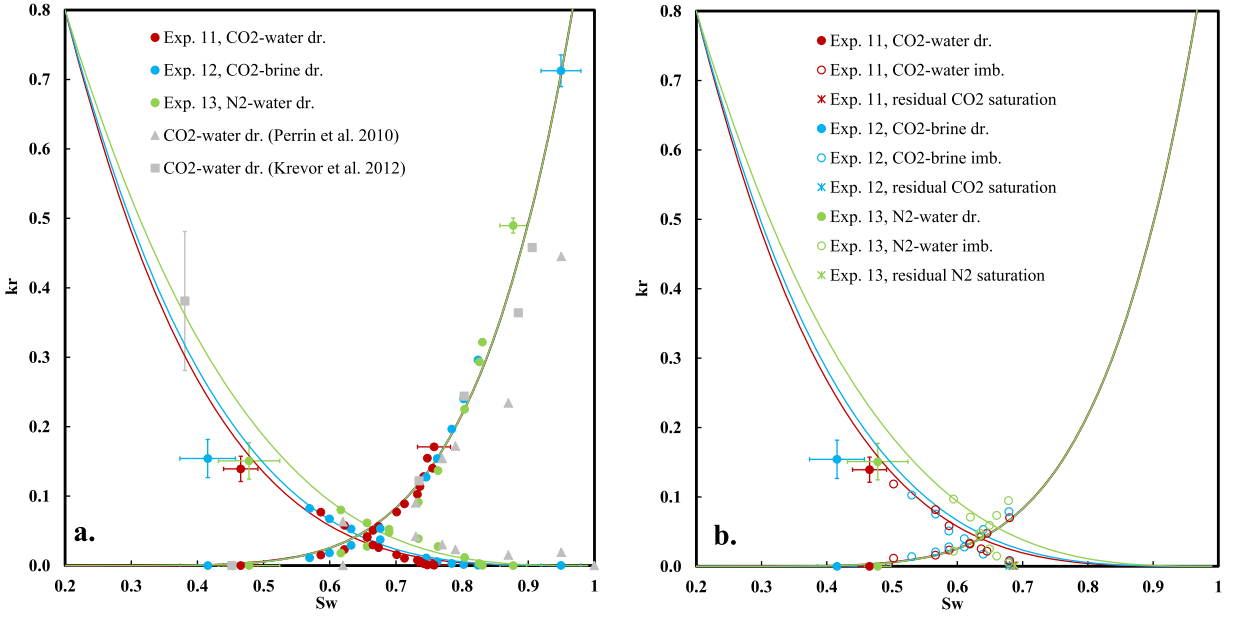

Figure 13. Steady state (a) drainage and (b) imbibition relative permeability. Solid lines are Brooks-Corey curves fit to the data and an arbitrary endpoint value for the nonwetting phase. Residual saturation corresponding to the drainage turnaround in Figure 13b are shown on the horizontal axis. See the text and Table 1 for details.

Small differences in the data scaled by the *J*-function in the comparison with *Pentland et al*. [2011] and *Pini and Benson* [2013] were likely due to differences in the rock properties. The observations from this work were consistent, however, with observations reported by *Pentland et al*. [2011]; *Pini et al*. [2012]; and *Pini and Benson* [2013] in consolidated Berea sandstone, in which the comparison of drainage capillary pressure characteristic curves between CO_2-brine and a separate fluid pair were found to scale with interfacial tension alone. This is also consistent with the conclusions in *Egermann et al*. [2006] that drainage core flood displacements of brine by supercritical CO_2 could be predictively modeled based on a characterization of flow properties with other fluid systems, e.g., N_2-water and mercury-air.

This suggests that the sensitivity of the wetting state observed in sessile and pendant drop contact angle measurements [*Chiquet et al*., 2007; *Espinoza and Santamarina*, 2010; *Jung and Wan*, 2012; *Wang et al*., 2012; *Kim et al*., 2012; *Broseta et al*., 2012] and in unconsolidated sand [*Plug and Bruining*, 2007; *Tokunaga et al*., 2013; *Wang and Tokunaga*, 2015] has little impact during drainage in consolidated sandstone. This observation was also supported by the results of the drainage and imbibition relative permeability tests, discussed below, which showed little variation between test conditions.

3.1. The Impact of Pressure, Temperature, and Brine Salinity on Capillarity

Experiments, 1, 7, and 8, performed at 5, 10, and 20 MPa, respectively, and 50°C and 0 M, were used to evaluate the effect of pressure on the wetting state. The characteristic curves are shown in Figure 9. The pressure range in the tests was such that the CO_2 phase was gaseous, low-density supercritical CO_2, and high-density supercritical CO_2 at the respective conditions (Figure 1). With increasing pressure, the interfacial tension between the fluids is reported to decrease from a range of 41–48 mN/m to a range of 24–30 mN/m, with the correlation of *Li et al*. [2012] showing a decrease from 47 to 30 mN/m, Table 1.

The data reflect the trend of increasing capillary strength with interfacial tension. Figure 9 shows the data scaled by the interfacial tension values reported in *Li et al*. [2012] alongside the curve fit scaled by the full range of interfacial tension values found in the literature at similar conditions (Table 1). The observations scaled with interfacial tension, including the observations made with the N_2-water system. This was indicative of no observable difference in multiphase flow due to impacts on the wetting state, both among conditions and in comparison to the water wet N_2 system.

The impact of temperature can be observed comparing Experiments 1, 3, 5, and 6 performed at 25 and 50°C, with the CO_2 phase in a liquid or supercritical state. Two pairs of experiments were performed at these conditions—one with deionized water (Experiments 1 and 5) and one with a 3 mol kg^{-1} NaCl solution (Experiments 3 and 6). In the deionized water systems, the interfacial tension increased from a reported range of 28–34 mN/m to a range of 30–36 mN/m with the increase in temperature. In the systems with NaCl in solution, the interfacial tension increased from a reported range of 29–38 mN/m to 35–41 mN/m.

The characteristic curves are shown in Figure 10, including the curve for the N_2-water system. A plot is again shown scaling the data by the interfacial tension values of *Li et al*. [2012] and the Brooks-Corey curves with the full range of reported values. In this case the observations do not strictly show an increase in capillary strength with interfacial tension. At each salinity, increasing the temperature, and the corresponding transition from liquid to supercritical CO_2, resulted in a small weakening of the capillary strength despite the corresponding, albeit small, increase in interfacial tension. This effect was small, however, and within the range of uncertainty with respect to the values of the interfacial tension. Comparison with the N_2-water curve again suggested that the systems were water wet.

The impact of salinity can be observed by comparing the results of Experiments 1, 2, 3, and 4 in in which the salinity varied from deionized water, to 5 mol kg^{-1} NaCl, at constant temperature and pressure. In this case, the interfacial tension varied from a range of reported values of 30–36 mN/m with deionized water to a range of 44–46 mN/m in the 5 molal solution.

The characteristic curves are shown in Figure 11 and exhibit an increasing capillary strength with increasing interfacial tension. There is more variation, however, in the CO_2-brine data than expected from effects of

interfacial tension alone. The Brooks-Corey curves fit to the data are shown scaled by the full range of interfacial tension values reported at a given salinity. Variation in the reported values of interfacial tension does not substantially resolve the difference in the scaled curves. It is thus possible that there was some sensitivity in the wetting character of the system with salinity. In this case, increasing salinity corresponded to an increasingly water wet system. All of the data were clustered around the data from the N_2 system and thus the displacement was still characteristic of a water wet drainage process.

3.2. Evaluating the Wetting State

The most variation among data scaled by the interfacial tension was observed with variation in salinity. To quantify shifts in this data, possibly due to wetting, we used a constant multiplier, ξ, the Arabic letter "Ayn," such that scaling $P_c/(\sigma\xi)$ collapsed the data to a single curve. A value of ξ was given to the N_2-water P_c curve to serve as the reference water wet system.

The scaled data are shown in Figure 12. A list of best fit values of ξ for the scaling is shown in Table 4. Values of $\xi > 1$ suggested that a system was more strongly water wet than the N_2-water system and $\xi < 1$ indicated that a system was less strongly water wet. As is clear from the preceding discussion of the results, the possible effects of wetting are small. The multiplier ranges from a value of $0.77 < \xi < 1.43$. This indicates that potential wetting effects were limited to result in a maximum decrease in capillary pressure at a given saturation by a factor of about 2 between the systems with the strongest and weakest capillarity, respectively.

3.3. Drainage Relative Permeability

The results of the drainage relative permeability tests are shown in Figure 13a. Axial saturation maps and averaged saturation profiles are provided in Appendix D and showed that the fluids were uniformly distributed for observations at every fractional flow, and not strongly affected by capillary end effects for all except the injection of 100% CO_2 at the end of the drainage cycle. As is common for studies with CO_2 and other low viscosity gases, the irreducible water saturation at the capillary endpoint to drainage was not achieved. This is because the achievable capillary pressure is limited in core floods by the maximum viscous pressure gradient that can be obtained in the core [*Krevor et al*., 2012]. Thus endpoint parameters for the Brooks-Corey models were assumed at values that have been obtained in past studies using Berea sandstone, e.g., *Oak et al*. [1990]. The Corey parameters were the only fitting parameters and suggest that there was little impact of changing conditions and fluid pairs.

The two drainage relative permeability curves for CO_2-brine were indistinguishable from each other, consistent with the observation that there was little impact of wetting state changes on capillarity with changes in brine salinity. The data for the N_2-water curve fall to the right of the CO_2-brine observations. This could be indicative of a difference in wetting between the fluids [*Berg et al*., 2013], but could also be caused by subtle effects that the interplay between rock heterogeneity and interfacial tension can have on observations of relative permeability [*Krause*, 2012; *Kuo and Benson*, 2013]. Subsequent observations at higher fluid flow rates are currently being undertaken to determine this. The crossover point of the curves are above the 50% water saturation mark, characteristic of drainage in water wet systems [*Craig*, 1971]. As with the capillary pressure data, the findings were consistent with those of *Egermann et al*. [2006] which reported that relative permeability for N_2-brine systems could be used to model drainage in CO_2-brine core floods, so long as the thermophysical properties were taken into account.

3.4. Imbibition Relative Permeability

Observations of imbibition relative permeability are shown in Figure 13b for the CO_2-brine and N_2-water tests. The imbibition tracking curve is dependent on the saturation turnaround point at the end of drainage, which was different for the three experiments. Thus the hysteresis tracking curves themselves were not directly comparable. However, initial-residual data for these conditions were reported in a separate study on the same rock by *Niu et al*. [2015]. Using the maximum saturation obtained at the end of drainage as the turnaround point, the estimated residual saturations are shown on the horizontal axis in Figure 13b. The hysteresis tracking curves approach the predicted value of the residual. That study found the IR curve to be equivalent for CO_2-brine and N_2-brine systems, and invariant across a range of reservoir conditions. Thus the imbibition tracking curves obtained for this work were consistent with imbibition governed by water wet displacement physics. Further observations of imbibition processes, particularly of the capillary

pressure-saturation relationship during imbibition in consolidated rocks should be a high priority for further investigation.

4. Conclusions

This study investigated the impact of conditions of pressure, temperature, and brine salinity on the drainage capillary pressure characteristic curve of CO_2-brine systems in sandstone. Eight capillary pressure tests were performed in a Berea sandstone at a range of conditions that were generally representative of the range of conditions in target CO_2 storage reservoirs worldwide.

Observed variation between the capillary pressure curves were largely explained by the corresponding variation in interfacial tension at those conditions, suggesting little impact of a change in wetting state. A comparison with the water wet N_2-water system also showed the CO_2-brine systems to be water wet.

The only variation in the scaled capillary pressure curves that exceeded the range of uncertainty from reported values of interfacial tension was seen with salinity variation from 0 to 5 molal NaCl brine solutions. In this case, the observed variation resulted in a maximum strengthening of capillarity (shifting upward of the capillary pressure curve) at the highest salinity of a factor of two over the system with dieonized water.

The observations were complemented with steady state drainage and imbibition relative permeability observations in CO_2-brine systems at 0 and 3 mol kg^{-1} NaCl. The drainage curves for CO_2 and brine at the two conditions were indistinguishable but slightly shifted with respect to a set of N_2-water curves. Imbibition curves exhibited hysteresis and were consistent with the characterization of the initial-residual characteristic of the rock previously published in *Niu et al.* [2015], consistent with water-wet displacement physics during imbibition in Berea sandstone.

Appendix A: Experimental Procedure

The first stage in each experiment was to remove air from the flow loop by flowing CO_2 through all parts of the experimental setup at an elevated pressure and released to the atmosphere. This was done at different stages by isolating different sections of the flow loop to insure that air was removed entirely. The system was then pressurized with CO_2 and heated to the experimental pressure and temperature. This step was required to obtain the CO_2 saturated core background scan. Next, water or brine, depending on the experimental fluid, was injected into the loop to displace and dissolve all of the CO_2 out of the core at the experimental pressure and temperature. A scan of the brine-saturated core was obtained for porosity measurements.

The absolute permeability to water was measured before each experiment. Permeability was measured by injecting water or brine, based on the experimental fluid, through the core sample at different constant flow rates and recording the pressure drop across the core. Permeabilities varied less than 5% throughout the series of tests suggesting minimal or no changes (i.e., fines migration, chemical reaction) in the core sample throughout the entire course of experiments performed in this study.

Water and CO_2 were circulated at experimental conditions in a closed loop bypassing the core. Carbon dioxide dissolved into the water until equilibration was reached. This resulted immiscible displacement. The dissolution of CO_2 into water was monitored by observing the mass balance of the fluid phases. The equilibration process started with a decreasing trend of the free-phase CO_2 in the system with subsequent stabilization of the phase confirming fluid equilibration. Equilibrium was generally established in this setup after 6 h of circulating the fluids at constant flow rates of 20 mL min^{-1}. Circulation was continued for at least 12 h. At this point, the CO_2 flow was stopped and only CO_2 equilibrated brine was circulated to ensure all free CO_2 was pushed through the lines to the two phase separator. Then the CO_2 equilibrated brine was injected through the line into the core. Several pore volumes of brine were injected into the core sample to displace the initial brine with brine equilibrated with CO_2. This was confirmed by taking X-ray scans during injection until a slight increase in CT number corresponding to the higher density brine was observed. Once

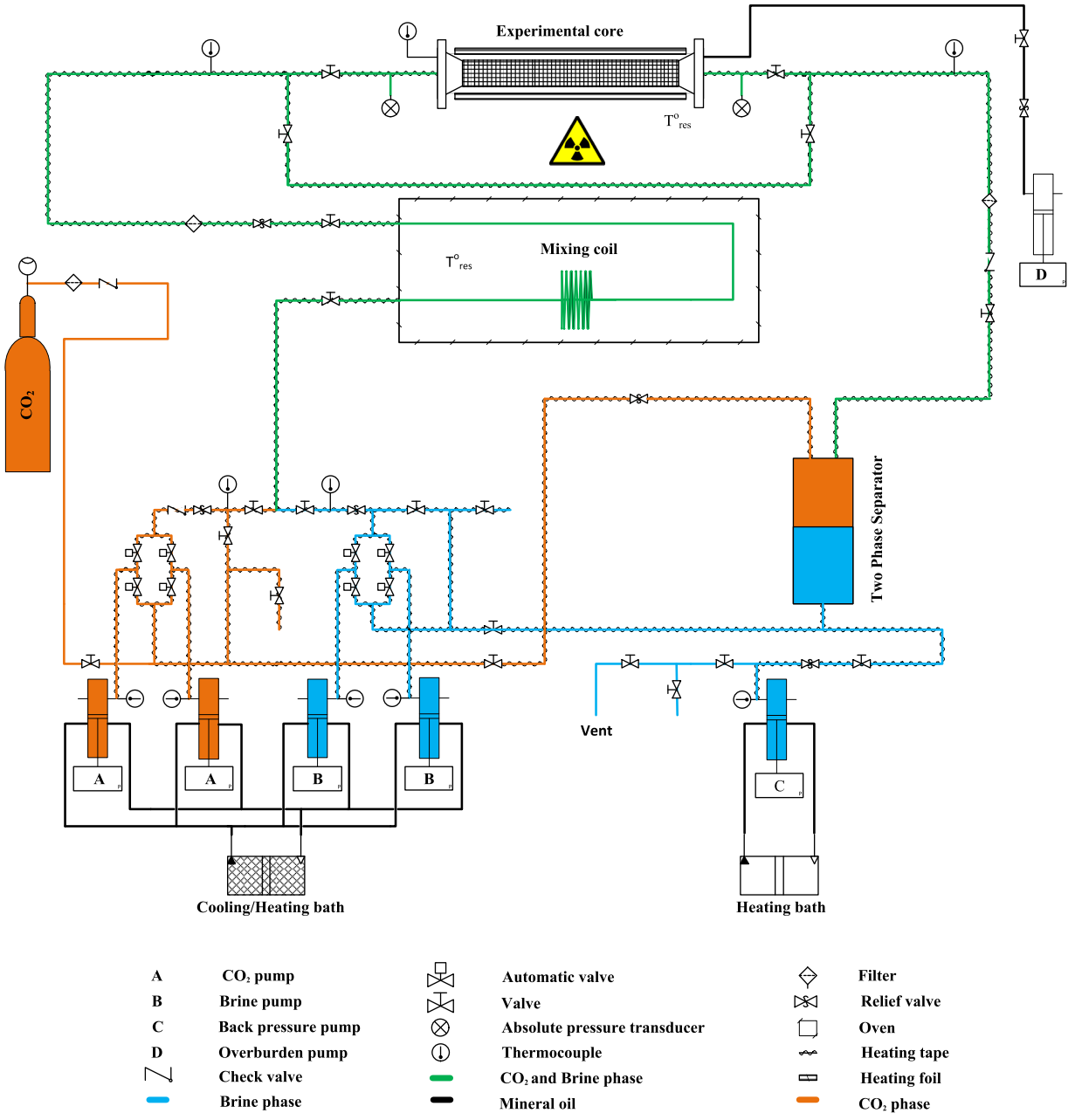

Figure A1. A schematic of the core flooding apparatus used in this study.

the core was fully saturated with CO_2 equilibrated brine, another background X-ray CT scan of the core was taken. At this stage, capillary pressure or relative permeability tests were performed.

The capillary pressure observations were initiated by injecting CO_2 into the core. For each capillary pressure measurement, CO_2 was injected at a constant flow rate until a constant pressure drop across the core was reached. Then, an X-ray scan was performed at the inlet face of the core sample. As described earlier, 10 scans over 10–30 s were taken of the inlet slice and then averaged for each saturation measurement to reduce the uncertainty associated with the computed saturations.

All steady state relative permeability experiments were performed at a constant total volumetric rate of 15 mL min^{-1}. The total volumetric flow rates were kept constant while changing the fractional flow. End effects were evident in the extreme fractional flows and these data points tend to have large error bars.

Appendix B: Porosity and Fluid Saturation From X-ray Imaging

Porosity and experimental fluid saturations were measured under each experimental condition. Both porosity and saturation measurements were obtained by a combination of background and experimental X-ray scans [*Akin and Kovscek*, 2003; *Withjack*, 1988]. The X-ray imaging parameters applied in this study were as follows: a voxel dimension of about (0.23 × 0.23 × 1) mm^3, a display field of view of 12 cm, an energy level of the radiation of 120 keV, and a tube current of 200 mA. The porosity was measured using four sets of X-ray scans. The first two were one scan of the air and one scan of the experimental brine at ambient conditions. The brine scans were made for every experiment so that the CT number of each particular brine-saturated core was obtained. The third scan was a scan of the dry core at ambient conditions where the pore space was filled with air. The fourth was a scan of the core saturated with brine at experimental conditions. The same confining pressure was applied in last two scans. The porosity was then calculated using

$$\phi = \frac{CT_{brine} - CT_{dry}}{I_{brine} - I_{air}} \tag{B1}$$

where CT and I were the X-ray CT scanner attenuation coefficient converted to numerical values in Hounsfield units. These values were assigned for each voxel in the X-ray image. The parameters CT_{brine} and CT_{dry} were CT numbers from the brine-saturated core and the dry core, respectively. The parameters I_{brine} and I_{air} were CT numbers obtained from scanning brine and air alone, respectively.

Fluid saturation measurements in the core sample required two background scans in addition to the experimental scan. The background scans were one scan of the core saturated with CO_2 and one scan of the core saturated with CO_2-equilibrated brine. Both scans were taken at experimental conditions and with confining pressure. Carbon dioxide saturation during CO_2 flow was calculated using

$$S_{CO_2} = \frac{CT_{\exp} - CT_{brine+CO_2}}{CT_{CO_2} - CT_{brine+CO_2}}, \tag{B2}$$

where the subscripts *exp*, CO_2, and $brine+CO_2$ refer to scan values obtained during CO_2 injection through the core during core-flooding, when the core was saturated with CO_2 and when the core was saturated with CO_2 equilibrated brine, respectively. The slice-averaged porosity and saturation properties were calculated using slice-averaged CT numbers. A total of 10 scans were taken for each set of CT numbers used in equations (B1) and (B2). The repeated scans were then averaged to reduce the uncertainty associated with the computed porosities and saturations.

Appendix C: Experimental Design Using a Numerical Simulator

Numerical simulation was used to estimate drainage flow rates that would result in even coverage of data across a range of capillary pressures and saturations achievable within the flow rate limitations of the experimental apparatus. We describe this model in detail here but emphasize that the simulation was simply used to analyze the assumptions underlying the technique and to aid with the initial choice of fluid flow rates, not to interpret the experimental observations. A model of the rock core was constructed for use in the adaptive implicit-explicit black oil simulator (IMEX) from the computer modeling group (CMG). The fluids CO_2 and brine were immiscible by default in the black oil simulator, consistent with the conditions created in the experiments in this work. The simulations were performed on a two-dimensional homogeneous model constructed to represent an axial slice from the middle of the Berea sandstone rock core. The model had 200 grid cells along the flow direction and 50 in the vertical direction. This corresponded to the minimum image thickness obtained from our CT scanner and allowed us to anticipate the potential impact of gravity segregation. The Brooks-Corey model, equations (D2) and (D3), was used to describe the relative permeability using data from experiments reported in *Krevor et al*. [2012]. The capillary pressure characteristic curve was estimated from the MICP data scaled to the CO_2-brine system using the Young-Laplace scaling, equation (1), ignoring the contact angle term. The mercury-air interfacial tension applied was 485 mN/m [*Ritter and Drake*, 1945]. After conversion, the data were fit with the

Brooks-Corey model, equation (2), for use in the simulator. Boundary slices were added to both inlet and outlet ends of the core, having the same dimension and properties as the rock slices following a similar procedure outlined in *Kuo and Benson* [2013]. Constant injection rate-controlled wells and constant bottom hole pressure controlled wells were completed in the grid elements of the inlet and outlet boundary slices, respectively. In addition, linear relative permeabilities were used for the inlet and outlet slices to allow full mobility for each phase. The capillary pressure between CO_2 and brine was set to zero at the inlet. For the outlet boundary condition, the capillary pressure was set to a constant equal to the entry capillary pressure. This arrangement produced simulation results most consistent with our observations of the impact of the inlet and outlet boundaries.

Appendix D: Steady State Relative Permeability Measurement Technique and Saturation Maps

Three steady state relative permeability tests were performed in this work to complement the findings from the capillary pressure characteristic curve tests. The one-dimensional form of the

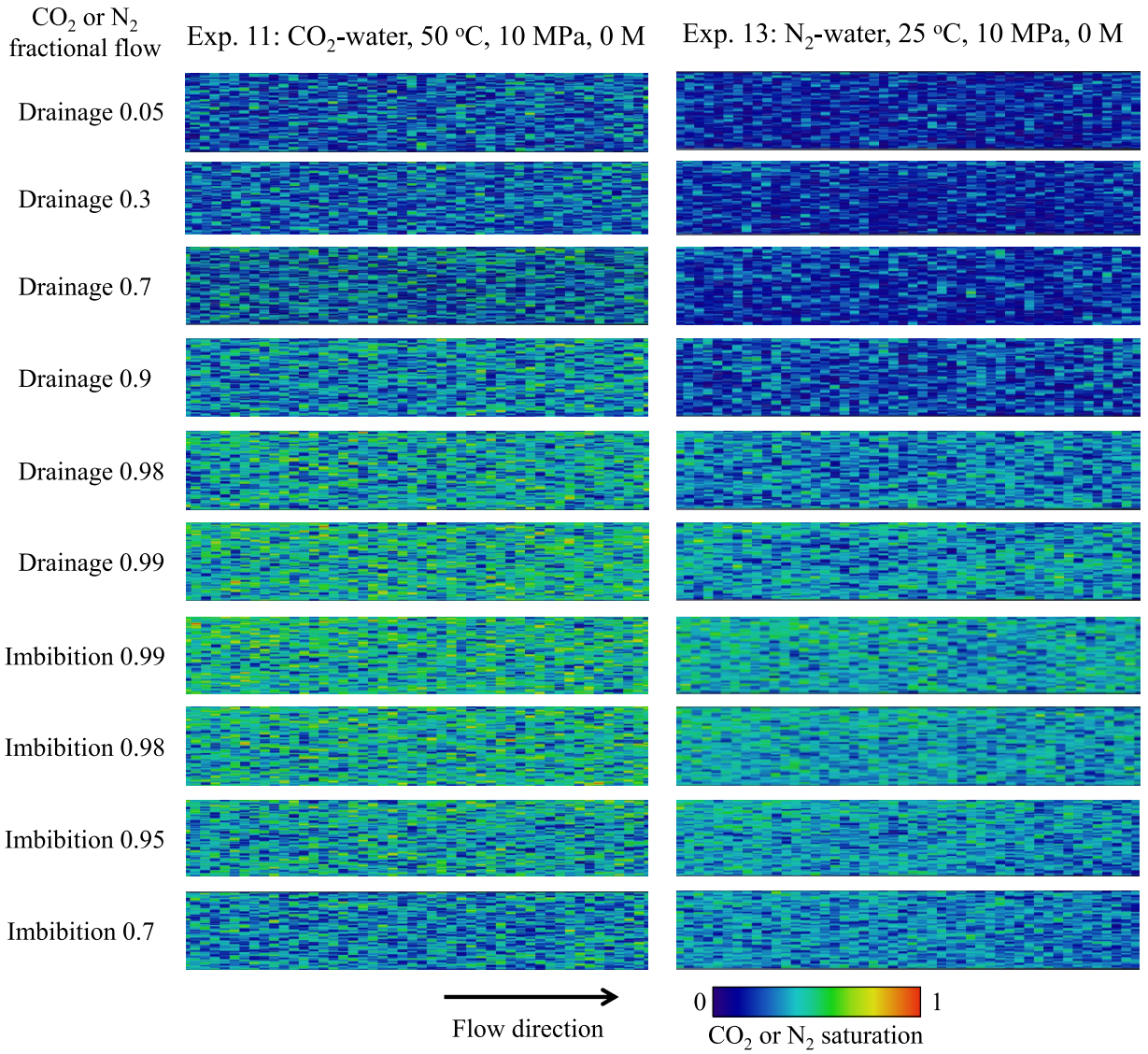

Figure D1. Vertical-horizontal central cross-sectional slice saturation maps of CO_2 and N_2 for some of the fractional flows applied to measure steady-state relative permeability Experiments 11 and 13, respectively.

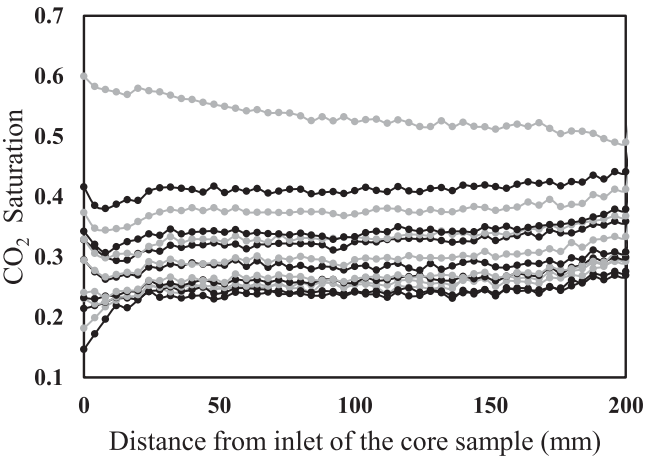

Figure D2. Slice-averaged CO_2 saturation profiles along the length of the core at 15 cm^3 min^{-1} at different fractional flows in a steady state relative permeability experiment of CO_2-water at 10 MPa and 50°C.

extended Darcy's law [*Dullien*, 1991] was used to calculate the relative permeability at a given fractional flow.

$$q_1 = -\frac{Akk_{r,1}(S_1)}{\mu_1}\frac{\Delta P_1}{\Delta x} \tag{D1}$$

where q_1 is the volumetric flow rate of a particular phase, A is cross sectional area of the core sample, k is the absolute permeability, $k_{r,1}(S_1)$ is the phase relative permeability as a function of its saturation, μ_1 is the phase viscosity, Δx is the length of the core, and ΔP is pressure drop across the core.

The saturation in the core sample was controlled by the ratio of injected phases (i.e., the fractional flow). In this study, in situ saturation was measured along the entire sample with X-ray CT for each fractional flow once a constant pressure drop (i.e., steady state) was achieved. For the drainage test, CO_2 saturation was incrementally increased from zero by increasing the fractional flow, f_{CO_2}. The fractional flow was controlled by simultaneously changing the relative volumetric flux of CO_2 and water while holding the total volumetric flow rate ($q_{CO_2}+q_{water}$) constant. Axial saturation maps and averaged saturation profiles are shown in Figures D1, D2 and D3.

The Brooks-Corey model was fit to the drainage relative permeability observations [*Brooks and Corey*, 1964]

$$k_{r,w} = k_{r,w}(S_{nw,r})\left(\frac{s_w - s_{w,irr}}{1 - s_{w,irr} - s_{nw,r}}\right)^{n_w} \tag{D2}$$

$$k_{r,nw} = k_{r,nw}(S_{w,irr})\left(\frac{1 - s_w - s_{nw,r}}{1 - s_{w,irr} - s_{nw,r}}\right)^{n_{nw}}. \tag{D3}$$

The parameters n_w and n_{nw} are unit less fitting parameters for wetting and nonwetting phase curves, the subscripts *nw* and *w* refer to the nonwetting and wetting phase, respectively, $k_{r,w}(S_{nw,r})$ and $k_{r,nw}(S_{w,irr})$ are the corresponding relative permeability endpoints.

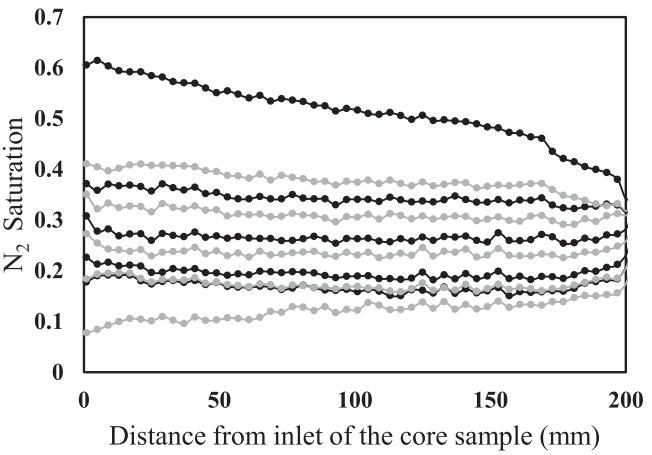

Figure D3. Slice-averaged N_2 saturation profiles along the length of the core at 15 cm^3 min^{-1} at different fractional flows in a steady state relative permeability experiment of N_2-water at 10 MPa and 25°C.

Acknowledgments
The authors thank four anonymous reviewers and the editors of Water Resources Research for their time and valuable comments which led to important improvements on earlier drafts of the work. This research has been performed as a part of the Qatar Carbonates and Carbon Storage Research Centre at Imperial College London. The authors gratefully acknowledge funding for the Centre provided jointly by Qatar Petroleum, Shell and the Qatar Science & Technology Park. All experimental data and simulation results used in this paper are accessible by contacting the corresponding author at a.al-menhali12@imperial.ac.uk.

References

Akin, S., and A. Kovscek (2003), Computed tomography in petroleum engineering research, *Geol. Soc. Spec. Publ.*, *215*(1), 23–38.
Al-Menhali, A., B. Niu, and S. Krevor (2015), The impact of reservoir conditions on wetting and multiphase flow properties measurements for CO_2-brine-rock system during primary drainage, in *International Symposium of the Society of Core Analysts SCA2015-018*, Newfoundland and Labrador, Society of Core Analysts, Canada, 16–20 Aug.
Amott, E. (1959), Observations relating to the wettability of porous rock, *Trans. Am. Inst. Min. Metall. Pet. Eng.*, *216*, 156–162.
Anderson, W. (1987), Wettability literature survey-part 4: Effects of wettability on capillary pressure, *J. Pet. Technol.*, *39*(10), 1283–1300.
Bachu, S. (2003), Screening and ranking of sedimentary basins for sequestration of CO_2 in geological media in response to climate change, *Environ. Geol.*, *44*(3), 277–289.
Bachu, S., and D. B. Bennion (2009), Interfacial tension between CO_2, freshwater, and brine in the range of pressure from (2 to 27) MPa, temperature from (20 to 125) °C, and water salinity from (0 to 334 000) mg L^{-1}, *J. Chem. Eng. Data*, *54*, 765–775.
Bachu, S., W. Gunter, and E. Perkins (1994), Aquifer disposal of CO_2: Hydrodynamic and mineral trapping, *Energy Convers. Manage.*, *35*(4), 269–279.
Berg, S., S. Oedai, and H. Ott (2013), Displacement and mass transfer between saturated and unsaturated CO2-brine systems in sandstone, *Int. J. Greenhouse Gas Control*, *12*, 478–492.
Bernstein, L., P. Bosch, O. Canziani, Z. Chen, R. Christ, O. Davidson, W. Hare, S. Huq, D. Karoly, and V. Kattsov (2007), IPCC, 2007: Climate Change 2007: Synthesis report, in *Contribution of Working Groups I, II and III to the Fourth Assessment Report of the Intergovernmental Panel on Climate Change*, edited by Core Writing Team, R. K. Pachauri and A. Reisinger, Intergov. Panel on Climate Change, Geneva. [Available at http://www.ipcc.ch/ipccreports/ar4-syr.htm.]
Brooks, R., and A. Corey (1964), *Hydraulic Properties of Porous Media, Hydrology Papers*, vol. 3, Colo. State Univ., Collins.
Broseta, D., N. Tonnet, and V. Shah (2012), Are rocks still water-wet in the presence of dense CO2 or H2S?, *Geofluids*, *12*(4), 280–294.
Chalbaud, C., M. Robin, J.-M. Lombard, F. Martin, P. Egermann, and H. Bertin (2009), Interfacial tension measurements and wettability evaluation for geological CO_2 storage, *Adv. Water Resour.*, *32*, 98–109.
Chiquet, P., D. Broseta, and S. Thibeau (2007), Wettability alteration of caprock minerals by carbon dioxide, *Geofluids*, *7*(2), 112–122.
Chun, B.-S., and G. T. Wilkinson (1995), Interfacial tension in high-pressure carbon dioxide mixtures, *Ind. Eng. Chem. Res.*, *34*(12), 4371–4377.
Craig, F. F. (1971), *The Reservoir Engineering Aspects of Waterflooding*, Soc. of Pet. Eng., N. Y.
Cuiec, L. (1975), Restoration of the natural state of core samples, paper *SPE 5634-MS* presented at *Fall Meeting of the Society of Petroleum Engineers of AIME*, Soc. of Pet. Eng. Dallas, Tex.
De Witt, L., and J. Schölten (1975), Studies on pore structure of adsorbents and catalysts: Iii. Comparison of pore size distributions determined in chrysostile and zirconia samples by mercury porosimetry and nitrogen capillary condensation, *J. Catal.*, *36*, 36–47.
Decker, E., B. Frank, Y. Suo, and S. Garoff (1999), Physics of contact angle measurement, *Colloids Surf. A*, *156*, 177–189.
Donaldson, E., R. Thomas, and P. Lorenz (1969), Wettability determination and its effect on recovery efficiency, *SPE J.*, *9*(1), 13–20.
Doughty, C., and K. Pruess (2004), Modeling supercritical carbon dioxide injection in heterogeneous porous media, *Vadose Zone J.*, *3*, 837–847.
Dullien, F. A. (1991), *Porous Media: Fluid Transport and Pore Structure*, Academic, Waterloo, Ontario, Canada.
Dumore, J., and R. Schols (1974), Drainage capillary-pressure functions and the influence of connate water, *Soc. Pet. Eng. J.*, *14*(05), 437–444.
Edenhofer, O., R. Pichs-Madruga, Y. Sokona, E. Farahani, S. Kadner, K. Seyboth, A. Adler, I. Baum, S. Brunner, and P. Eickemeier (2014), IPCC, 2014: Climate change 2014: Mitigation of climate change, *IPCC Working Group III*, Transport, Geneva, Switzerland.
Egermann, P., C. Chalbaud, J.-P. Duquerroix, and Y. Gallo (2006), An Integrated approach to parameterize reservoir models for CO_2 injection in aquifers, paper *SPE 102308 presented at Society of Petroleum Engineers Annual Technical Conference and Exhibition*, Society of Petroleum Engineers, San Antonio, Tex., 24–27 Sept.
Espinoza, D. N., and J. C. Santamarina (2010), Water-CO_2-mineral systems: Interfacial tension, contact angle, and diffusion–implications to CO_2 geological storage, *Water Resources Research*, *46*, W07537, doi:10.1029/2009WR008634.
Farokhpoor, R., B. Bjorkvik, E. Lindeberg, and O. Torsaeter (2013), Wettability behavior of CO_2 at storage conditions, *Int. J. Greenhouse Gas Control*, *12*, 18–25.
Fordham, E. J., L. D. Hall, T. S. Ramakrishnan, M. R. Sharpe, and C. Hall (1993), Saturation gradients in drainage of porous media: NMR imaging measurements, *AIChE J.*, *39*(9), 1431–1443.
Foster, W. (1973), A low-tension waterflooding process, *J. Pet. Technol.*, *25*(2), 205–210.
Global CCS Institute (2014), *The Global Status of CCS: 2014*, Docklands, Victoria, Australia.
Georgiadis, A., G. Maitland, J. P. M. Trusler, and A. Bismarck (2010), Interfacial tension measurements of the ($H_2O + CO_2$) system at elevated pressures and temperatures, *J. Chem. Eng. Data*, *55*(10), 4168–4175.
Golding, M. J., J. A. Neufeld, M. A. Hesse, and H. E. Huppert (2011), Two-phase gravity currents in porous media, *J. Fluid Mech.*, *678*, 248–270.
Golding, M. J., H. E. Huppert, and J. A. Neufeld (2013), The effects of capillary forces on the axisymmetric propagation of two-phase, constant-flux gravity currents in porous media, *Phys. Fluids*, *25*(3), 036602.
Good, R. J., and R. S. Mikhail (1981), The contact angle in mercury intrusion porosimetry, *Powder Technol.*, *29*(1), 53–62.
Gupta, S. P., and S. P. Trushenski (1979), Micellar flooding-compositional effects on oil displacement, *SPE J.*, *19*(2), 116–128.
Hesse, M., F. M. Orr Jr., and H. Tchelepi (2008), Gravity currents with residual trapping, *J. Fluid Mech.*, *611*, 35–60.
Iglauer, S., M. Fernø, P. Shearing, and M. Blunt (2012), Comparison of residual oil cluster size distribution, morphology and saturation in oil-wet and water-wet sandstone, *J. Colloid Interface Sci.*, *375*(1), 187–192.
Iglauer, S., A. Salamah, M. Sarmadivaleh, K. Liu, and C. Phan (2014), Contamination of silica surfaces: Impact on water-CO_2-quartz and glass contact angle measurements, *Int. J. Greenhouse Gas Control*, *22*, 325–328.
Iglauer, S., C. Pentland, and A. Bush (2015), CO_2 wettability of seal and reservoir rocks and the implications for carbon geosequestration, *Water Resour. Res.*, *51*, 729–774, doi:10.1002/2014WR015553.
International Energy Agency (2012), *IEA World Energy Outlook 2012*, Paris, France.
Jadhunandan, P. P., and N. R. Morrow (1995), Effect of wettability on waterflood recovery for crude-oil/brine/rock systems, *SPE Reservoir Eng.*, *10(1)* 40–46.
Jerauld, G., and J. Rathmell (1997), Wettability and relative permeability of Prudhoe bay: A case study in mixed-wet reservoirs, *SPE Reservoir Eng.*, *12(1)*, 58–65.

Juanes, R., E. Spiteri, F. M Orr Jr., and M. Blunt (2006), Impact of relative permeability hysteresis on geological CO_2 storage, *Water Resour. Res.*, *42*, W12418, doi:10.1029/2005WR004806.
Jung, J.-W., and J. Wan (2012), Supercritical CO_2 and ionic strength effects on wettability of silica surfaces: Equilibrium contact angle measurements, *Energy Fuels*, *26*(9), 6053–6059, doi:10.1021/ef300913t.
Kim, Y., J. Wan, T. J. Kneafsey, and T. K. Tokunaga (2012), Dewetting of silica surfaces upon reactions with supercritical CO_2 and brine: Pore-scale studies in micromodels, *Environ. Sci. Technol.*, *46*(7), 4228–4235.
Krause, M. (2012), Modeling and investigation of the influence of capillary heterogeneity on relative permeability, paper *SPE-160909-STU presented at Society of Petroleum Engineers Annual Technical Conference and Exhibition*, Society of Petroleum Engineers, San Antonio, Tex., 8–10 Oct.
Krevor, S. C. M., R. Pini, L. Zuo, and S. M. Benson (2012), Relative permeability and trapping of CO_2 and water in sandstone rocks at reservoir conditions, *Water Resour. Res.*, *48*, W02532, doi:10.1029/2011WR010859.
Kruyer, S. (1958), The penetration of mercury and capillary condensation in packed spheres, *Trans. Faraday Soc.*, *54*, 1758–1767.
Kuo, C.-W., and S. M. Benson (2013), Analytical study of effects of flow rate, capillarity, and gravity on CO_2/brine multiphase-flow system in horizontal corefloods, *SPE J.*, *18*(4), 708–720.
Lenormand, R., A. Eisenzimmer, and C. Zarcone (1993), A novel method for the determination of water/oil capillary pressures of mixed-wettability samples, paper presented at Society of Core Analyst Conference 9322, Houston, Tex.
Levine, J. S., D. S. Goldberg, K. S. Lackner, J. M. Matter, and M. G. Supp (2014), Relative permeability experiments of carbon dioxide displacing brine and their implications for carbon sequestration, *Environ. Sci. Technol.*, *48*(1), 811–818.
Li, X., E. Boek, G. C. Maitland, and J. P. M. Trusler (2012), Interfacial tension of (brines + CO_2): (0.864 NaCl + 0.136 KCl) at temperatures between (298 and 448) K, pressures between (2 and 50) MPa, and total molalities of (1 to 5) mol kg^{-1}, *J. Chem. Eng. Data*, *57*(4), 1078–1088, doi:10.1021/je201062r.
McCaffery, F. G., and D. W. Bennion (1974), The effect of wettability on two-phase relative penneabilities, *J. Can. Pet. Technol.*, *13*(4), 42–53.
Morrow, N. R. (1976), Capillary pressure correlations for uniformly wetted porous media, *J. Can. Pet. Technol.*, *15*(4), 49–69.
Niu, B., A. Al-Menhali, and S. Krevor (2015), The impact of reservoir conditions on the residual trapping of carbon dioxide in Berea sandstone, *Water Resour. Res.*, *51*, 2009–2029, doi:10.1002/2014WR016441.
Nordbotten, J., and H. Dahle (2011), Impact of the capillary fringe in vertically integrated models for CO_2 storage, *Water Resour. Res.*, *47*, W02537, doi:10.1029/2009WR008958.
Oak, M., L. Baker, and D. Thomas (1990), Three-phase relative permeability of Berea sandstone, *J. Pet. Technol.*, *42*(8), 1054–1061.
Orr, F. (2004), Storage of carbon dioxide in geologic formations, *J. Pet. Technol.*, *56*(9), 90–97.
Pentland, C. H., R. El-Maghraby, S. Iglauer, and M. J. Blunt (2011), Measurements of the capillary trapping of super-critical carbon dioxide in Berea sandstone, *Geophys. Res. Lett.*, *38*, L06401, doi:10.1029/2011GL046683.
Pini, R., and S. M. Benson (2013), Simultaneous determination of capillary pressure and relative permeability curves from core-flooding experiments with various fluid pairs, *Water Resour. Res.*, *49*, 3516–3530, doi:10.1002/wrcr.20274.
Pini, R., S. C. M. Krevor, and S. M. Benson (2012), Capillary pressure and heterogeneity for the CO_2/water system in sandstone rocks at reservoir conditions, *Adv. Water Resour.*, *38*, 48–59, doi:10.1016/j.advwatres.2011.12.007.
Plug, W. J., and J. Bruining (2007), Capillary pressure for the sand-CO_2-water system under various pressure conditions: Application to CO_2 sequestration, *Adv. Water Resour.*, *30*(11), 2339–2353.
Purcell, W. R. (1949), Capillary pressures: Their measurement using mercury and the calculation of permeability therefrom, *J. Pet. Technol.*, *1*(2), 39–48.
Ramakrishnan, T. S., and A. Cappiello (1991), A new technique to measure static and dynamic properties of a partially saturated porous medium, *Chem. Eng. Sci.*, *46*(4), 1157–1163, doi:10.1016/0009-2509(91)85109-B.
Ritter, H., and L. Drake (1945), Pressure porosimeter and determination of complete macropore-size distributions, *Ind. Eng. Chem. Anal. Ed.*, *17*(12), 782–786.
Salathiel, R. (1973), Oil recovery by surface film drainage in mixed-wettability rocks, *J. Pet. Technol.*, *25*(10), 1216–1224.
Saraji, S., L. Goual, M. Piri, and H. Plancher (2013), Wettability of supercritical carbon dioxide/water/quartz systems: Simultaneous measurement of contact angle and interfacial tension at reservoir conditions, *Langmuir*, *29*, 6856–6866.
Swanson, B. (1985), Microporosity in reservoir rocks-its measurement and influence on electrical resistivity, in *SPWLA 26th Annual Logging Symposium*, *Soc. of Petrophys. and Well-Log Anal*, Society of Petrophysicists and Well-Log Analysts, *26*(6), 42–52.
Szulczewski, M. L., C. W. MacMinn, H. J. Herzog, and R. Juanes (2012), Lifetime of carbon capture and storage as a climate-change mitigation technology, *Proc. Natl. Acad. Sci. U. S. A.*, *109*(14), 5185–5189.
Taber, J. (1969), Dynamic and static forces required to remove a discontinuous oil phase from porous media containing both oil and water, *SPE J.*, *9*(01), 3–12.
Tokunaga, T. K., J. Wan, J.-W. Jung, T. W. Kim, Y. Kim, and W. Dong (2013), Capillary pressure and saturation relations for supercritical CO_2 and brine in sand: High-pressure $P_c(s_w)$ controller/meter measurements and capillary scaling predictions, *Water Resour. Res.*, *49*, 4566–4579, doi:10.1002/wrcr.20316.
Wang, S., and T. K. Tokunaga (2015), Capillary pressure: Saturation relations for supercritical CO_2 and brine in limestone/dolomite sands: Implications for geologic carbon sequestration in carbonate reservoirs, *Environ. Sci. Technol.*, *49*(12), 7208–7217, doi:10.1021/acs.est.5b00826.
Wang, S., I. M. Edwards, and A. F. Clarens (2012), Wettability phenomena at the CO_2–brine–mineral interface: Implications for geologic carbon sequestration, *Environ. Sci. Technol.*, *47*(1), 234–241.
Warwick, P. D., et al. (2013), National assessment of geologic carbon dioxide storage resources: Results, *U.S. Geol. Surv. Circ., 1386*, 41 pp.
Withjack, E. (1988), Computed tomography for rock-property determination and fluid-flow visualization, *SPE Form. Eval.*, *3*(4), 696–704.
Wu, S., and A. Firoozabadi (2010a), Permanent alteration of porous media wettability from liquid-wetting to intermediate gas-wetting, *Transp. Porous Media*, *85*, 189–213.
Wu, S., and A. Firoozabadi (2010b), Effect of salinity on wettability alteration to intermediate gas-wetting, *SPE Reservoir Eval. Eng.*, *13*(2), 228–245.
Yan, W., G.-Y. Zhao, G.-J. Chen, and T.-M. Guo (2001), Interfacial tension of (methane + nitrogen) + water and (carbon dioxide + nitrogen) + water systems, *J. Chem. Eng. Data*, *46*, 1544–1548.